Available online at www.sciencedirect.com
SCIENCE DIRECT
Polymer 46 (2005) 10854–10865
polymer
www.elsevier.com/locate/polymer

Hierarchical morphology of carbon single-walled nanotubes during sonication in an aliphatic diamine

Janis M. Brown[a,*], David P. Anderson[b], Ryan S. Justice[c], Khalid Lafdi[b], Max Belfor[c], Karla L. Strong[a], Dale W. Schaefer[c]

[a]*Air Force Research Laboratory, Materials and Manufacturing Directorate, MLBCO, WPAFB, OH 45433-7750, USA*
[b]*University of Dayton Research Institute, 300 College Park, Dayton, OH 45469-0168, USA*
[c]*Department of Chemical and Materials Engineering, University of Cincinnati, Cincinnati, OH 45221-0012, USA*

Received 11 January 2005; received in revised form 10 August 2005; accepted 31 August 2005
Available online 29 September 2005

Abstract

Dispersion of single-walled carbon nanotubes (SWNTs) by sonication into diamine curing agents is studied as a means to improve the dispersion of SWNTs in cured epoxy. Cured and uncured specimens are analyzed by light microscopy, electron microscopy, light scattering (LS), ultra small-angle X-ray scattering (USAXS), electrical conductivity and Raman spectroscopy. A flexible diamine (D2000) forms a stable SWNT suspension leading to good homogeneity in both the diamine and the cured epoxy. High resolution transmission electron microscopy (TEM) shows that small ropes of SWNTs (mostly under 15 nm) are present despite the sample's visual homogeneity. Further morphological investigation of cured and uncured D2000 resins using light and small-angle X-ray scattering indicates that the SWNTs are networked into fractal clusters that electrically percolate at low SWNTs loadings (0.05 wt%).
Published by Elsevier Ltd.

Keywords: Small-angle scattering; Single-walled carbon nanotubes; Hierarchical morphology

1. Introduction

Single-walled carbon nanotubes (SWNTs) have great promise as nanofillers or perhaps even as nanoreinforcements for composites. Observed reinforcement is well below the order-of-magnitude improvement one might hope to see from SWNTs. This discrepancy in mechanical properties has been attributed to poor SWNT dispersion [1], poor load transfer due to low rope shear modulus [2] due to slipping within the ropes [3], poor load transfer to the interior of the ropes [4], the fractal nature of ropes leading to low effective modulus [5], poor load transfer due to poor chemical bonding between the resin and the SWNT [6], and process-related deficiencies leading to low filler volume and voids. Recent calculations by Liu and Kumar [7] emphasize that high modulus nanocomposites require either high levels of orientation or exfoliation (dispersion).

For reasons such as the above, good dispersion of SWNTs is vital to achieve high-modulus nanocomposites. Since performance is dependent on many factors, however, it is essential to have some measure of degree of SWNT exfoliation other than composite mechanical properties. In this work, we use light scattering (LS), ultra-small angle scattering (USAXS), microscopy and spectroscopy to characterize the morphology and dispersion of SWNTs in both the amine curing agent and the amine-cured epoxy.

Since SWNTs, exfoliated or not, rapidly increase the viscosity of resins, SWNT-loaded epoxies can be difficult to process. A typical method applied to both nanoclays in epoxy [8] and SWNTs in polyimides [9] to overcome this limitation uses a compatible solvent that is later removed from the SWNT/epoxy system (solvent-assist). In contrast, we disperse SWNTs into a neat liquid diamine (melt processing), avoid the use of solvent, and eliminate additional processing steps associated with solvent removal.

The exact nature of the attractive interaction of SWNTs with nitrogen-containing compounds such as amines is the subject of ongoing debate. Some investigators report a charge transfer interaction between the nitrogen and the SWNT, specifically an electron donation from the nitrogen to the SWNT [10–15]. Hydrogen bonding [16] between ammonia and the SWNT has also been reported. Steric hindrance of interaction between the SWNT and the amine may determine which polymers stabilize

* Corresponding author. Tel.: +1 937 255 0968; fax: +1 937 656 4706.
E-mail address: janis.brown@wpafb.af.mil (J.M. Brown).

0032-3861/$ - see front matter Published by Elsevier Ltd.
doi:10.1016/j.polymer.2005.08.089

more effectively [14,15]. Pi orbital interaction may be involved if there are aromatic rings in the structure [17,18]. Still others propose a copolymer compatibilization between the SWNT and a variety of block copolymers in organic or aqueous solvents [15,19,20].

Furthermore, SWNTs may form charge-transfer complexes with amines that change the electrical properties of SWNTs [10,11,13,21]. Semi-conducting SWNTs were combined with the highly aminated protein streptavidin [11], with an amine-rich polymer polyethyleneimine (PEI) [21], ammonia [10] and various alkyl amines [13,22]. In all cases, SWNTs readily absorb (for the polymers irreversibly) the amine-containing compounds either as a gas or in solution. Finally, Choi and co-workers [23] reported that *n*-butylamine and aniline added to SWNTs in DMF aid in unbundling of SWNTs.

Furtado [24] reported debundling acid-cleaned arc-grown SWNTs at very low concentrations (0.02 mg/ml) after low-power bath sonication in DMF or *N*-methyl pyrrolidone (NMP) followed by 20,800*g* centrifugation. These conditions are less aggressive than the 540-W sonication and 125,000*g* centrifugation used by O'Connell [25,26], Moore [19,27], and Islam [28] to disperse SWNTs into surfactant solutions. AFM confirmed 50% yield of small (1.4–2 nm) tubes in the HCl/DMF/NMP-treated SWNTs after sonication and/or centrifugation. Furtado observes that for the HCl/NMP or DMF samples centrifugation does not dramatically affect the yield of small tubes and proposes that few large bundles are left after the low-power sonication. The debundling and dispersion did not occur for as-received samples of SWNTs that had not been acid treated. The hydrochloric acid may also intercalate the ropes allowing amide access to the interior. The amide intercalation is facilitated by ultrasound and charge transfer between the amide and the SWNTs.

Other nanoscale carbonaceous materials such as vapor grown carbon nanofibers (VGCNF) [29] as well as carbon black [30–32] have been reported to be stabilized by mixing in liquid diamines prior to the addition of epoxy. Loadings of 1–10 wt% VGCNFs, which are at least an order of magnitude larger diameter than SWNTs, were predispersed by sonication into the diamine D2000 prior to addition of a bisphenol A-type epoxy (Epon 828) which resulted in samples showing good dispersion. Carbon black dispersions are also stabilized as 500-nm aggregates by sonication in an aromatic liquid diamine Araldite HY 932 with a Bisphenol A type epoxy [30,32]. Therefore, it seems reasonable that similar methods could be used to achieve good dispersion of SWNTs.

Researchers at Cambridge [33–35] successfully utilized the procedure originally proposed by Jager [36], Richard [29], Flandin [30], and Schueler [32] for the stabilization of VGCNF and carbon black to suspend multi-walled nanotubes (MWNTs) in epoxy resin. For electrostatic discharge and electromagnetic charge interference protection, Sandler and coworkers [33] added MWNTs into epoxy forming a three-dimensional conductive carbon network. Very low percolation thresholds (0.0225 and 0.04 wt%) were achieved with conductivity as high as 10^{-2} S-cm^{-2}. Several years later, Sandler et al. [35] successfully used this approach to produce an extremely low percolation threshold at 0.0025-wt% using initially aligned CVD MWNTs.

Martin and coworkers [33–35] recently demonstrated the importance of processing protocol for dispersion of MWNTs. MWNTs were dispersed in an aromatic-amine-cured DGEBA epoxy using various processing conditions. The multi-walled nanotubes formed visible, >1 μm, clusters. The cluster size was a function of mixing temperature, shear rate, and final cure temperature. Cluster formation was tracked by increases in conductivity.

The studies reviewed above suggest a processing path exists for SWNT-reinforced epoxy using a liquid diamine curing agent as a carrier. In this work, we demonstrate this idea using long-chain diamines.

2. Experimental

SWNTs manufactured by the HiPco™ process [37] were supplied by Rice University (HiPco™ Batch 87) and cleaned according to Strong [38] using hydrochloric acid, which removes most of the iron catalyst. We avoided sulfuric and nitric acids to limit oxidation of the SWNTs. With the hydrochloric acid treatment, there is a small amount of adsorbed molecular oxygen (about 1-mol%) on the SWNTs, but we do not observe the formation of carbon-oxygen products in X-ray photoelectron spectroscopy (not shown) nor do we see a carbonyl peak in the FTIR spectra.

Short-chain diamines (D230 and D400) of the Jeffamine series (from Huntsman LLC) were used for initial photomicrographs (Fig. 1). D230 and D400 are liquid short-chain polyoxypropylene diamines with $n=3$ and $n=5.6$, respectively. All resin castings were made using the long-chain Jeffamine D2000, a liquid, aliphatic polyoxypropylene diamine with a nominal degree-of-polymerization of 33. Castings were made with 0.01-g of clean SWNTs added to 7.25-g of D2000. The SWNT/D2000 mixture was sonicated with a Fisher Model 60 Dismembrator sonicator with a 3-mm diameter titanium horn. Samples were made using sonication times of 30 min, 1, 2, and 4 h. During sonication, the temperature of the mixtures rose to 65–90 °C. After sonication, 2.75 g of heated (75 °C) epoxy (Epon 828, a bisphenol A diglycidyl ether from Miller-Stephenson) was then added to the SWNT/D2000 mixture. In the case of conventional mixing, the mixture was stirred and cast at this point. Other formulations were sonicated for an additional hour at 75 °C after adding the epoxy to form the prepolymer during the sonication. The samples were placed in a heated 75 °C mold and cured for 2 h at 75 °C followed by 2 h at 125 °C.

Micro-Raman spectroscopy was performed with a Renishaw Raman microscope at room temperature. Samples were excited using a 3-mW Ar^+ laser operating at 830 nm (1.496 eV). A 20× objective lens with 10 s exposure induces no damage on liquid or solid samples. Calibration was performed with the Si band at 520.7 cm^{-1}. Raman bands were fit with a Lorentzian line shape. No attempt was made to normalize the intensity of the peaks, as normalization may mask a decrease in intensity due to functionalization or

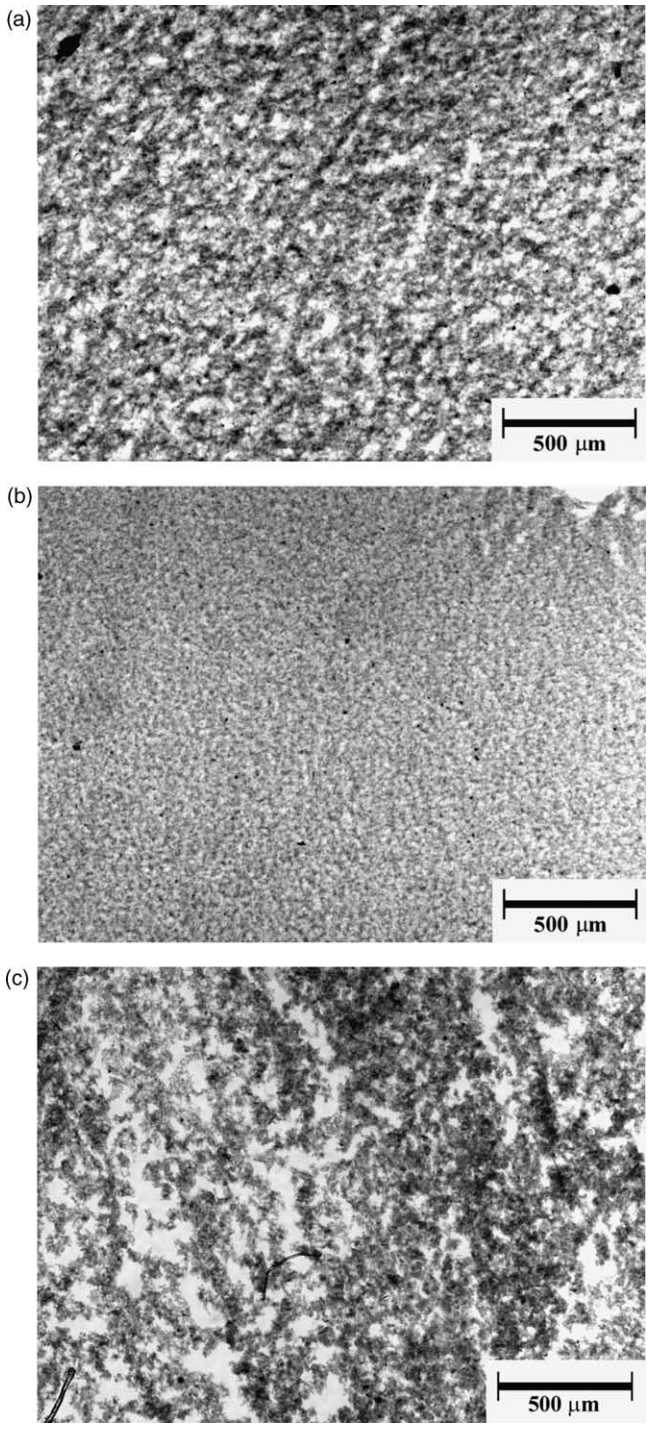

Fig. 1. Light microscopy of SWNTs in Jeffamine D-2000, sonicated at 10 W for (a) 15 min, (b) 60 min, and (c) in Jeffamine D-400 for 60 min.

charge transfer. The error in the peak positions was less than $\pm 1.5\ cm^{-1}$.

Raman of liquid samples was performed by placing the liquid in a small holder and shining the laser directly down into the liquid, focusing slightly below the surface. This methodology prevents artifacts due to the presence of a glass or plastic sample holder. An attempt was made to perform Raman spectroscopy using 514.5 nm, but the effects of solvent fluorescence overpowered the SWNT spectrum.

For Raman spectroscopy, 0.1 wt% SWNTs were sonicated at 10 W for various times in 1% sodium dodecyl sulfate (NaDS) and distilled deionized water; sodium dodecyl benzene sulfonate (NaDDBS) in distilled deionized water; dimethyl formamide (DMF); and D2000. In this study, SWNTs were sonicated in each solvent and then immediately analyzed with Raman spectroscopy.

Suspensions of SWNTs in water-based sodium polystyrene sulfonate ($PSSO_3$, $M_w = 500{,}000$) were used for elucidation of the light scattering data. These samples were prepared as previously described [5,39]. The suspensions were studied using a Micromeritics 5200 Saturn Digisizer. Ultra small angle X-ray scattering (USAXS), data were obtained using the Bonse-Hart USAXS camera at the UNICAT beam line at the Advanced Photon Source at Argonne National Laboratory. Combined light and X-ray scattering data were interpreted using a unified model assuming fractal morphology [40–42] as discussed previously by Schaefer et al. [5] with regard to SWNTs.

Suspensions of tubes were examined with light microscopy on a Nikon FXL light microscope in transmission. Photomicrographs of the cured materials were obtained with a Hitachi S-5200 high-resolution scanning electron microscope (HR-SEM). Initial samples were cold fractured in liquid nitrogen and coated with 8 Å of Tungsten. Later samples were not coated and the resin was softened with the electron beam to expose SWNTs.

Transmission electron microscopy (TEM) sections of rubbery cured epoxy were prepared using cryo-ultramicrotomy. High quality imaging was possible by combining plunge-freezing and staining techniques. Samples were stained with osmium tetroxide to increase the image contrast.

In preparation for impedance measurements, 25 mm × 25 mm squares were cut from cast films of the SWNTs in Epon828/D2000. Silver was thermally evaporated on the squares using a Denton Explorer® 18 Cryo Auto High Vacuum Deposition System. The squares were sandwiched between two metal washers each with a 20-mm hole that served as a template for depositing circular silver plating on each side of the samples. The plating thicknesses were 1000 Å on each side. Impedance values were measured using a Novocontrol High Resolution Dielectric Analyzer. The Ac conductivity measurements were made over a frequency range between 10^{-2} and 10^{7} Hz at 25 °C. The AC output voltage was adjusted to 1 V. The silver-plated samples were placed between two gold-plated brass electrodes. The frequency dependence of the real part of the complex AC conductivity (σ'_{AC}) is reported.

DMA was run on solid cured samples using a Rheometric Scientific ARES 3A1 in torsion mode with 0.1% strain at 1 Hz from −145 °C (using liquid nitrogen coolant) to +100 °C.

3. Results and discussions

SWNT dispersion in the neat D2000 is a rather complex process. Without sonication the SWNTs do not disperse in either the epoxy or the diamine. With sonication in D2000, initially large chunks of SWNTs break up followed by

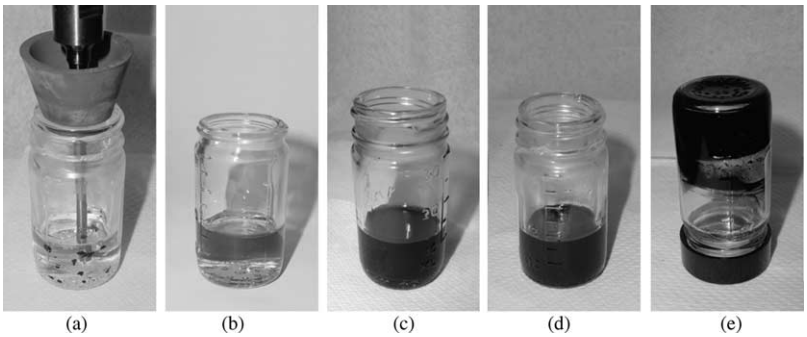

Fig. 2. Cleaned SWNTs in D2000 (a) prior to sonication, (b) 0.001 wt% sonicated 60 min 10 W, (c) 0.01 wt% sonicated 60 min 10 W, (d) 0.1 wt% sonicated 60 min 10 W, (e) 0.5% wt% gelled after sonication 60 min 10 W.

breakdown of agglomerates leading to greater homogeneity (Figs. 1 and 2). A period exists between 1 and 2 h of sonication (10 W) when the SWNT/D2000 suspensions become visually transparent and optically homogenous. The homogenous state is maintained for at least 120 min of sonication. After sonication ceases, reagglomeration leads to fluffy objects that eventually settle. This behavior is in contrast to the morphologies displayed in the short-chain aliphatic amines of the same series. SWNTs in D400 ($n=5.6$, Fig. 1(c)) and D230 ($n=3$, not shown), do not break up within the period of sonication (24 h), do not become transparent, and do not reform to fluffy agglomerates. The rest of this work, therefore, explores the more homogeneous SWNT/D2000 system. The superior performance of the D2000 compared to the lower molecular weight counterpart indicates that the amine with the longer alkyl moiety provides a combination of steric stabilization as well as attractive interaction between the SWNTs and the amine.

As shown in Fig. 2, with increasing concentrations of SWNTs (10 W sonication for an hour) the morphology changes from initial unswollen hard pellets of cleaned SWNTs to a low-viscosity gray clear liquid at 0.001 wt%, to a homogeneous transparent black liquid at 0.01–0.1 wt%, and to a physical gel at 0.5 wt% and above. All other samples were made at 0.1 or 0.14 wt% in diamine unless otherwise specified. The latter concentration gives a composite content of 0.1% when epoxy is added. Higher concentrations of SWNTs in diamine produced gel states, as did samples sonicated at higher powers for longer times. This gelation suggests that further dispersion is possible, but eventually network formation will limit the degree of dispersion that could be achieved. Gelation limits the loading of SWNTs to less than 0.4 wt% when neat diamine is used.

If there is a covalent reaction or a secondary interaction between the amine group and the SWNT, one would expect to see subtle effects in the amplitude and peak shifts within the Raman. Raman spectra were examined for the SWNT/D2000 system. Raman spectroscopy is highly sensitive to the electronic state of SWNTs, and therefore, is sensitive to any changes in the surface electronic state due to bonding or other interactions [43,44].

In order to determine the appropriate reference from which to measure peak shifts, a study was undertaken to compare Raman peak positions of dry SWNTs and suspensions of SWNT in a variety of solvent systems. The intent was to determine if Raman spectroscopy is sensitive to small charge transfers due to association with different functional groups. The solvents used were 1% sodium dodecyl sulfate (NaDS) and distilled deionized water, sodium dodecyl benzene sulfonate (NaDDBS) in distilled deionized water, DMF; diethyl diamine toluene (Cure agent W), and D2000. In order to minimize reversion to the bundled or charge-neutral state SWNTs were sonicated in each solvent for 1 h and then immediately analyzed with Raman spectroscopy. Fig. 3 shows the results of the study to find the appropriate reference for comparison of Raman spectrum peak shifts with changes in surface chemistry and environment. There is no difference in the G peaks between the amine samples, the surfactant samples, or the dry samples within the limits of resolution of the instrument ($\pm 1.5\ \mathrm{cm}^{-1}$).

Fig. 4 shows the Raman spectra for suspensions of SWNTs in D2000 sonicated for progressively longer periods of time. There are no changes in peak positions with increased sonication. Also, the relative intensities of the D and G peaks do not change, although the absolute intensities of both increased significantly at 2 h sonication, the opposite of what is expected with functionalization [45] or significant charge transfer [43,46,47].

These results show that the interaction of the amine with the SWNTs does not perturb the electronic structure enough to be detected by Raman. This observation is in agreement with

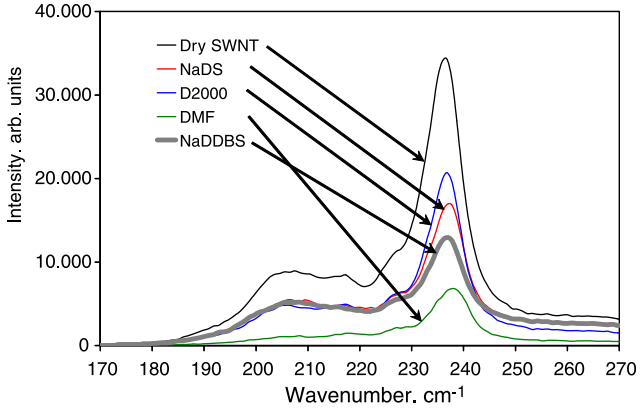

Fig. 3. Radial breathing mode region of the Raman spectra for various SWNT suspensions.

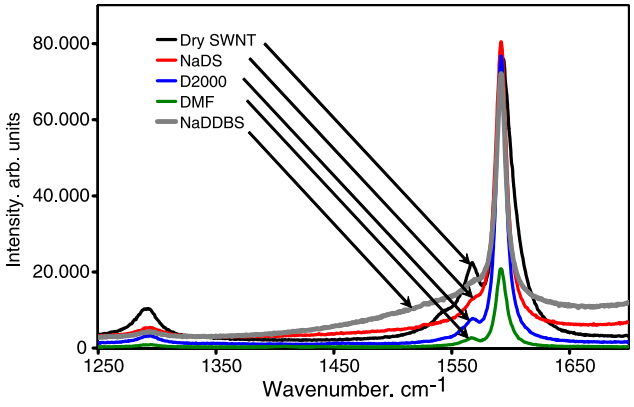

Fig. 4. D and G peak regions of the Raman spectra for various SWNT suspensions.

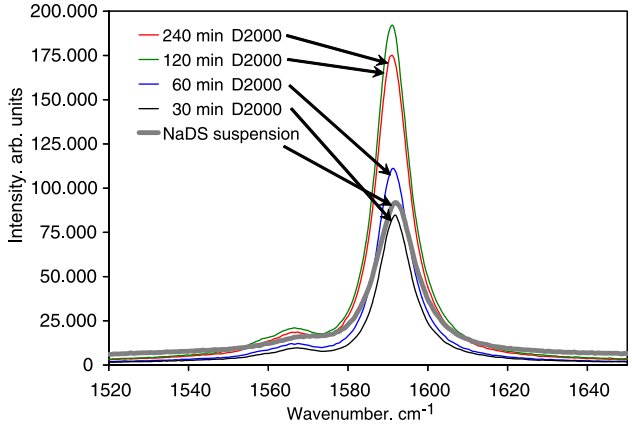

Fig. 5. Raman of SWNTs sonicated in D2000 diamine for 30, 60, 120, and 240 min. Spectra of SWNTs sonicated 60 min/10 W is NaDDBS is for reference.

the charge transfer of only 0.04 electrons per nitrogen calculated by Chang et al. [48], which gives a shift under 1 cm^{-1} [43,46,47] as well as the minimal effects shown by Heller et al. [49] for the G peak upon suspension into surfactant systems.

Fig. 5 shows the evolution of the Raman spectrum during sonication. The spectrum is typical save the extraordinary intensity maximum observed at 120 min sonication (at the same initial concentration). This increase in the peak intensity signals more nanotubes in smaller bundles than at other sonication times. Individual tubes are rare judging by the lack of fluorescence peaks in the higher wave number region [50]. A reduction of intensity at 240 min sonication time may be an indication of reagglomeration of the tubes into larger bundles. We see similar maxima in scattering between 1 and 2 h of sonication (below).

Ajayan [3] observed SWNT pull-out of a fractured epoxy matrix leaving a network of SWNT bundles on the surface. In the case of the samples studied here, however, we do not observe nanotubes or nanotube ropes on the cold-fractured surfaces at any magnification. As shown in Fig. 6, the SWNTs remain buried in the resin.

The SWNTs are difficult to visualize and some areas on the surface as they are unstable under the electron beam. Since the matrix is fragile, the SEM electron beam was used to create a fracture by local heating. After the matrix retracted (Fig. 7(a)), a large hole developed in the sample and all SWNT ropes that bridged the matrix network became visible (Fig. 7(a)). Some of the ropes are thin, ranging in size between 5 and 10 nm (Fig. 7(b)) and others were thicker between 10 and 50 nm (Fig. 7(b)). We did not observe any large ropes or bundles of ropes.

The SWNTs appear to be wetted by the polymer. In fact, they are thickly covered with polymer. The surfaces are quite different from dry pulled-out SWNTs typically seen on the fracture surface with unfunctionalized SWNTs or SWNTs not initially sonicated into the amine. In our case, the lack of SWNT pull-out is likely due to improved wetting [51]. Adhesion of the SWNT is probably due to a SWNT-amine complex formed during the initial sonication in the diamine. Further HiRES SEM and TEM were used to clarify the condition and the location of the SWNTs.

Fig. 8 shows a TEM image of SWNT ropes distributed in the rubbery epoxy matrix. There are well-distributed ropes between 10 and 20-nm thick in the matrix forming a network of SWNT ropes. To avoid experimental artifacts such as astigmatism, aberration etc. a real time FFT (fast fourier transform) was performed (inset in Fig. 8). The network of ropes can be seen in Fig. 9 as two ropes are merging into a single larger rope. Whether this merging is part of the separation of a thicker rope into several thinner ropes or the reagglomeration of thinner ropes is not known. What is clear is

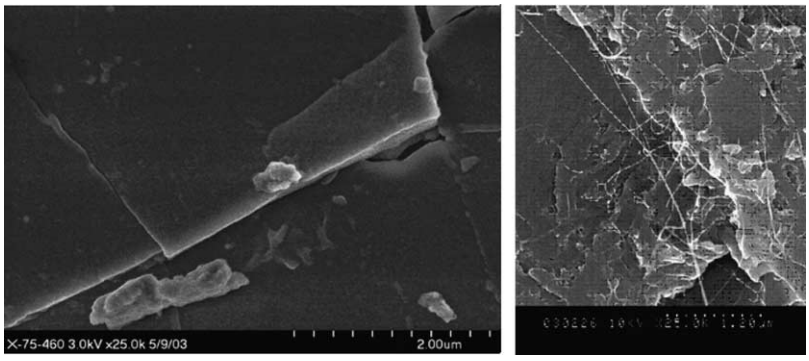

Fig. 6. HiRES SEM of SWNTs of fracture surfaces of diamine cured epoxy SWNTs sonicated in D2000 for 60 min cured with Epon 828. SWNTs are conventionally processed in Epon/Cure W (earlier sample from Brad Files at NASA Johnston). Note rope pull out in conventionally processed sample.

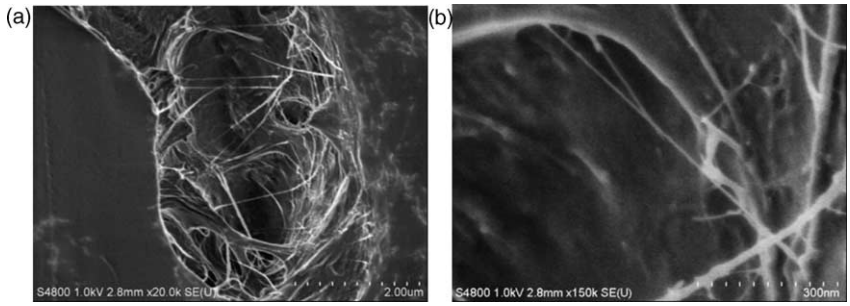

Fig. 7. SEM image of SWNTs in a rubbery epoxy made by sonicating the SWNTs for 60 min in Jeffamine D-2000 curing agent: (a) at lower magnification and (b) at higher magnification.

that isolated SWNTs are never observed and SWNT ropes merge or separate into a complex looped network.

Dynamic mechanical results for the cured samples are shown in Fig. 10. At this loading, there is no significant change in location (T_g) or breadth of the tan delta peak or in the 1-Hz glassy storage modulus (not shown). Of more interest is the 30–40% increase in storage modulus in the rubbery region. We see increases in the dynamic modulus even at loadings of 0.1 wt% well below the 1 wt% used by Gong [52] or the 1–10 wt% VCGNF used by Richard [29]. Concentrations above 0.4 wt% were not investigated because of network formation/gelation in the uncured amine made processing quite difficult.

A simple geometric calculation reveals that at 0.1 wt% the system is well above the rod percolation limit if the rods are fully dispersed with an aspect ratio of 1000 or larger. Using an aspect ratio of 1000 a space filling model for percolation developed by Garboczi, et al. [53] assuming a smooth, hard-surfaced prolate ellipsoids gives a percolation limit of approximately 0.092 wt% ($\phi = 0.0006$). This calculation is an upper limit based on hard ellipsoids. Considering that the SWNTs have the ability to aggregate, they may also form a network at a lower concentration. AC electrical measurements showed that the electrical percolation threshold was below 0.05 wt%, thus confirming that the SWNTs are networked at 0.1 wt%. Regardless of how well the original SWNT ropes are exfoliated at 0.1 wt%, the nanotubes will necessarily touch each other and given their proclivity to associate, the SWNTs will tend to reagglomerate into a network structure.

Fig. 11 is a log–log plot of the real part of the complex AC conductivity (σ'_{AC}) vs. frequency as a function of SWNT loading. At loadings ≤ 0.01 wt%, the composites show somewhat conductive behavior attributed to the pure epoxy resin, as the data from concentrations $\leq 0.01\%$ lay along the same values as the 0% SWNT sample (pure epoxy). As concentrations are increased to values $0.01\% < \text{wt}\% \leq 0.1\%$, the samples become more conductive. The first deviation we observe from the baseline resin conductivity occurs at 0.05 wt%. We attribute the jump in AC conductivity that occurs between $0.01 < \text{wt}\% \leq 0.05$ to a percolation transition, where the SWNTs form an electrically conductive network throughout the sample volume.

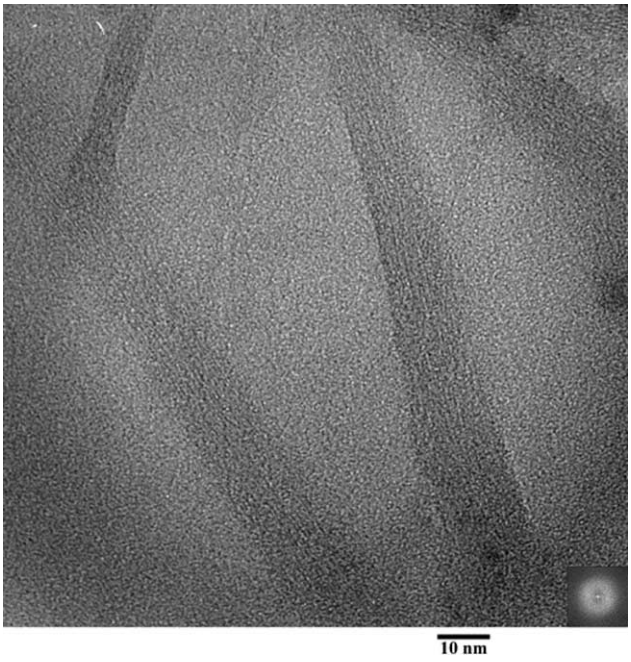

Fig. 8. TEM image of a SWNT rope in a rubbery epoxy matrix nanocomposite.

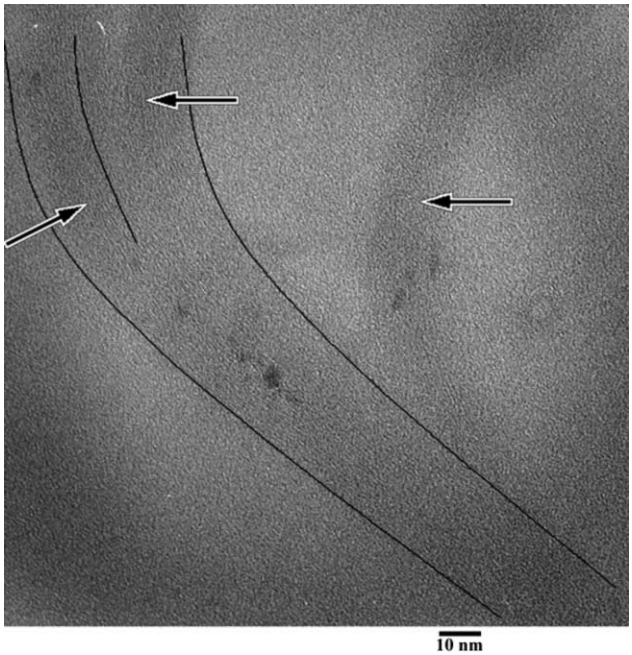

Fig. 9. TEM image of a SWNT rope in a rubbery epoxy matrix nanocomposite showing the separation of a larger rope into two thinner ropes.

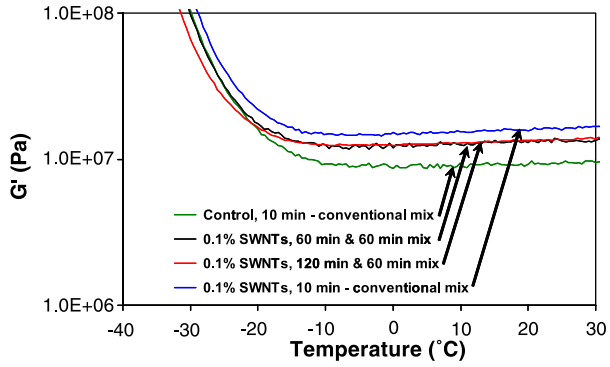

Fig. 10. DMA storage modulus data of some of the plaques in the rubbery region.

We were unable to establish a critical volume fraction (ϕ_c) because upon sonication, the amine dispersed SWNT samples gelled above 0.4 wt%. Thus we could not reach a concentration where the samples exhibit ohmic behavior. Since ohmic behavior is necessary to completely fit a percolation model, we can only determine a range where ϕ_c occurs. Ultimately, the range where we see the first substantial increase in σ'_{AC} is taken as ϕ_c. The data indicate 0.01 wt% $< \phi_c \leq$ 0.05 wt%.

The observed threshold is consistent with the literature. Rutkofsky et al. find percolation at 0.045 wt% in polystyrene ($\rho_{PS} = 1.05$ g/cm^3). As of April 2005 this value is the lowest percolation for a polystyrene composite [54]. Furthermore, Barrau et al. determined a percolation threshold of 0.3 wt% ($\phi_c = 0.002$) for carbon nanotubes ($\rho_{CNT} = 1.8$ g/cm^3) in a bisphenol A type epoxy resin ($\rho_{epoxy} = 1.2$ g/cm^3) [55]. Further illustrating consistency with the work of Barrau, they report ϕ_c to occur at $\sigma'_{AC} \sim 10^{-11}$ (S-cm^{-1}), which is consistent with the data in Fig. 11. Additionally, Koerner et al. using a DC four-point probe test and based on a simplified bond percolation model [56] reported network formation at 0.1 wt% ($\phi_c = 0.005$) for a dispersion of ASI carbon nanotubes ($\rho_{CNT} \sim 2.1$ g/cm^3) in polyurethane ($\rho_{polyureathane} \sim 1.19$ g/cm^3) [57]. Although the aforementioned list is not exhaustive, the values presented support a percolation threshold in the range 0.01 $<$ wt% $\leq$ 0.05%.

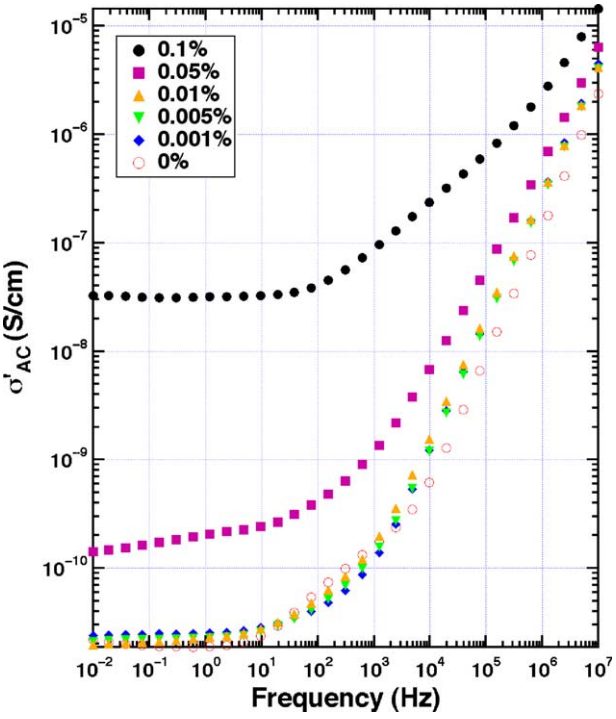

Fig. 11. Frequency dependence of the real part of the complex AC conductivity (σ'_{AC}) as a function of SWNT loading. The SWNT loadings are reported in carbon weight percentages.

To determine the nature and origin of this conductivity, light scattering and ultra small-angle X-ray scattering were used to characterize the morphology of SWNTs in amine curing agents and in cured epoxy. Compared to electron microscope imaging, scattering averages over a large sample volume ($>$0.9 mm^3) and therefore, is less sensitive to sampling errors. Scattering, on the other hand, provides information in reciprocal space and therefore, interpretation is model dependent.

Fig. 12 compares several light scattering profiles of SWNTs in D2000 and D230. The samples were externally sonicated for 30 min at 10 W and then observed under quiescent conditions (no sonication) in the non-circulating batch mode of the Micromeritics Saturn Digisizer light scattering photometer. Although the circulating mode is normally preferred to the batch mode (circulation guarantees more extensive averaging) circulation is not feasible with solids or high viscosity liquids.

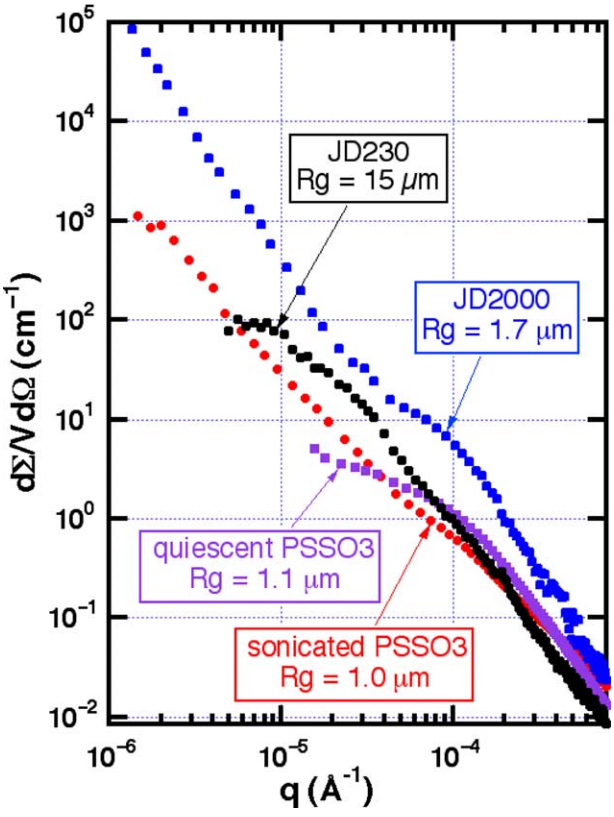

Fig. 12. Comparison of the light scattering data for SWNTs suspended in Jeffamine D-230 and Jeffamine D-2000 and in a PSSO3 solution. SWNT samples were externally sonicated and observed in the quiescent state 15 min after cessation of sonication.

The data are plotted as the relative intensity vs. q where q is the magnitude of the scattering vector. q is related to scattering angle as $q = (4\pi/\lambda)\sin(\theta/2)$, where θ is the scattering angle and λ is the wavelength in the medium. In this equation q is the reciprocal space variable conjugate to the spatial variable in the Fourier transform that relates the scattered intensity to the spatial correlation function. Thus, at a given q, scattering is sensitive to fluctuations in electron density on length scales of order q^{-1}.

Details on the interpretation of scattering data from carbon SWNTs are published elsewhere [5,39]. To summarize, SWNTs typically show rather featureless scattering profiles as in Fig. 12. To interpret these data it is useful to compare the results for SWNTs suspended in water using $PSSO_3$ as shown in Fig. 12. $PSSO_3$ is an effective suspension aid that yields a low viscosity water solution that can be observed using the Saturn Digisizer in the circulating mode. In $PSSO_3$, light scattering in the region $q < 1\times10^{-5}$ Å^{-1}, which we interpret as arising from bubbles generated by sonication, disappears on cessation of sonication as shown in the quiescent curve in Fig. 12.

In $PSSO_3$, the persistent scattering that remains after cessation of sonication is attributed to SWNTs. The profile consists of a so-called Guinier region where the data are approximately exponential ($2\times10^{-5} < q < 2\times10^{-4}$) followed by a power-law region with a power-law exponent (slope on a log–log plot) of -2.5. From the Guinier-region scattering we calculate that the scattering entities have a Guinier radius (radius-of-gyration for dilute systems) of 1.1 μm in $PSSO_3$. From the slope in the power-law region we conclude that the scatterers are fractal clusters of fractal dimension $=2.5$.

In both sonicated $PSSO_3$ and quiescent D2000, SWNT scattering appears as a shoulder on the dominant low-q scattering, which, in both cases, we attribute to scattering from bubbles whose size is too large to be resolved by the instrument. Using a multilevel fitting procedure [42] we can extract the Guinier radius of the feature attributed to SWNTs (1.7 μm for D2000 and 1.0 μm for sonicated $PSSO_3$).

If rod-like entitles were present, we would observe a power-law slope of -1 in the scattering profile [39]. Rather, in $PSSO_3$ we find micrometer-size fractal objects that are very likely microgel clusters consisting of a branched network of roped SWNTs. These systems are considered dispersed in the sense that they do not precipitate for days; however, the actual suspended carbon is aggregated into clusters. This interpretation is consistent with the light microscopy in Fig. 1.

Turning now to the interpretation of the amine-suspended carbon: the D230 (short chain diamine) data resemble the quiescent $PSSO_3$ in Fig. 12, so we use the same interpretation to deduce that there are 15 μm clusters of SWNT ropes. In this case there is no scattering from bubbles due to the relatively low viscosity of D230. This situation contrasts with the higher molecular weight and more viscous D2000 data, which show a shoulder corresponding to a radius-of-gyration of 1.7 μm as well as bubble-like scattering at low q. Overall we conclude that D2000 is a good dispersant since the cluster size is comparable to the smallest observed using a good suspension aid like $PSSO_3$ in water. Nevertheless, the carbon is not dispersed to the individual nanotube level.

Further evidence for the clustered nature of amine-suspended SWNTs comes from ultra-small angle X-ray scattering (USAXS). Unfortunately, at loading of 0.1%, SWNT scattering is rather weak. Nevertheless, after studying many systems some systematic observations emerge from the data. We studied scattering from 0.1 wt% carbon in both D2000 liquid and in D2000-cured Epon 828. The data are reported as the absolute differential scattering cross-section per unit sample volume. In all cases, an air-blank background was subtracted from the data.

Fig. 13 shows the evolution of the USAXS scattering profile as a function of sonication time. These samples were sonicated externally at either 10 or 120 W just prior to the USAXS data collection. The profiles show increasing intensity for times to 60 min. At 120 min sonication, however, the amplitude is less than at 60 min, possibly signaling re-agglomeration. We had previously observed re-agglomeration in water solution after prolonged sonication [5]. The key observation from these data is the gradual dispersion of carbon up to 60 min.

The shape of the scattering profiles (Fig. 13) contains information about the morphological state of the carbon. To assess the morphology, we subtract the scattering from the neat D2000 and display the background-subtracted results in Fig. 14. The 10-W sonication data show slopes of -2.4 at both low and high q with a knee separating the two regimes.

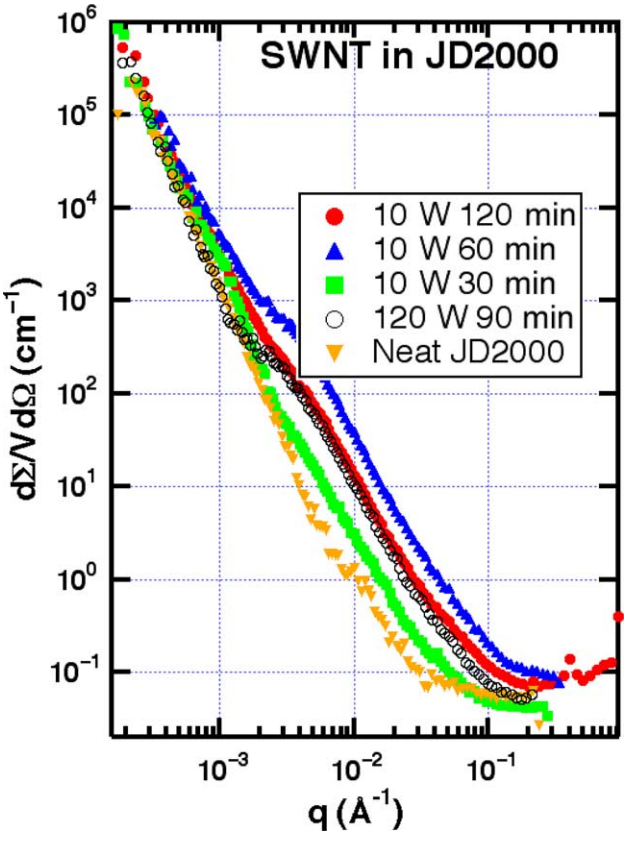

Fig. 13. USAXS data for 0.1 wt% SWNTs in Jeffamine D-2000 as a function of sonication time at 10 and 120 W. Maximum dispersion as judged by the amplitude of the scattering occurs at 60 min.

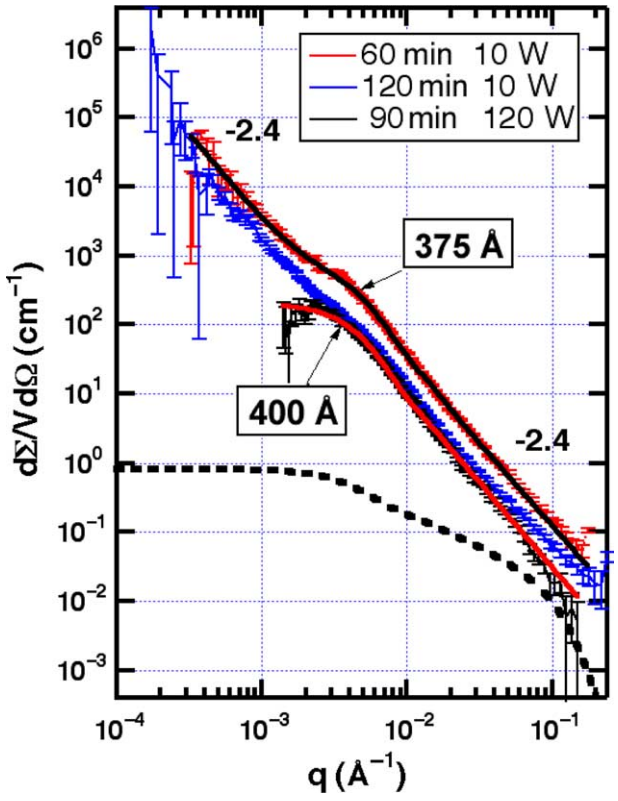

Fig. 14. Background-subtracted scattering data for SWNTs in Jeffamine D-2000. The solid lines through the 60 and 90 min data represent a one-level unified fit with the corresponding Guinier radii shown on the graph. All the data show a limiting high-q slope of about -2.4 corresponding to a fractal object. At low q the slope is also -2.4. The dotted line is the expected scattering for carbon rods 140 nm long and 4 nm diameter.

The 120-W sonication data show no scattering at small-q, but it must be realized that the subtraction errors in this region are quite large. All of the data show a length scale in the range 35–40 nm obtained from fitting the knee-region to a Guinier function using Beaucage's unified approach [42].

Interpretation of Fig. 14 is not obvious. One apparent feature, however, is absence of any region of slope of 1, the signature of a rod-like scatterer. The slopes of -2.4 are characteristic of fractal objects. This conclusion is similar to that reached regarding Fig. 12, albeit Fig. 12 refers to larger length scales compared to USAXS. Since the light scattering data in Fig. 12 also show limiting slopes close to -2.4, the USAXS data below 0.001 $Å^{-1}$ can be safely interpreted as arising from 1-μm clusters found in the light scattering data. The 40-nm length-scale and the high-q slope of -2.4 are more problematic. This slope implies a disorder within the ropes themselves. Based on the TEM observations (not shown) SWNTs can have rope diameters as large as 50-nm so this diameter can be from the ropes themselves. Based on the USAXS data, however, the concept of a rope is problematic. If there are remnants of the ropes seen in dry samples, the ropes are swollen and highly disordered. It should be emphasized that we do not have TEM data on the fluid D2000 sample for direct comparison.

An alternative interpretation of the 40-nm length scale is that it represents the 'mesh size' of the local SWNT network. To understand the meaning of the mesh size it is useful to consider scattering from a polymer gel. On length scales larger than the distance between crosslinks, a gel is uniformly dense, so scattering is flat in q-space. At smaller length scales (larger q), however, one observes scattering from the polymer chains that make up the gel, which typically give slopes of $\cong -2$ corresponding to a Gaussian chain. The crossover length scale between uniform and chain like scattering is the mesh size. The mesh size can also be thought of as the size of the holes in the network. Using this analogy, the SWNTs are the polymer chains and the distance between crosslinks is the distance between SWNT contact points.

To help with visualization of the possible hierarchical morphologies of SWNTs in D2000, described by the scattering above, a possible real space interpretation of these morphologies is given in Fig. 15. Two levels of hierarchy are represented. On large scales there is a network of ropes that accounts for the light scattering data. A second network of SWNTs is shown inside the ropes to account for the USAXS data. The mesh size of the large-scale network is about 1 μm and that of the small-scale network is about 40 nm.

Note that there is no evidence in the scattering behavior of isolated rods with linear morphology. To emphasize this fact, the predicted scattering from a carbon rod with diameter = 4 nm and length = 140 nm is shown in Fig. 14 at 0.1-wt% concentration. For these calculations a matrix density of 1 g/cm^3 and a carbon density of 1.4 gm/cm^3 and a chemical formula for D2000 of $C_{100}H_{209}O_{33.2}N_2$ were assumed. Even though the assumed diameter is larger than that on an isolated rod, the calculated results still fall orders of magnitude below the observed scattering, implying that, despite the visual uniformity of the samples, the SWNTs must aggregated into larger scale entities.

The scattered intensity drops considerably when the carbon is incorporated in the cured epoxy. As can be seen in Fig. 16, the resulting background-subtracted data lie only marginally above the unfilled background, giving rise to large subtraction errors. The lack of significant scattering is the result of the fact that the scattering-length density of carbon and cured E828 differ by only 5%, assuming the chemical formula of the cured system to be $C_{126}H_{236}O_{37.6}N_2$ with a density of 1 g/cm^3. The weak scattering in the epoxy confirms that the scattering does arise carbon.

The 60 min-SWNT/D2000 data from Fig. 14 are included in Fig. 16 for comparison. The most notable feature in the cured composite data is the absence of the 40-nm feature that is present in the SWNT/D2000 precursor. At the longest sonication time, the epoxy data show a gradual transition from a power-law slope of -3.4 at low q to a slope of -2.5 at large q. Once again it should be emphasized that the low-q data are subject to large subtraction errors. Overall, however, we conclude that the SWNT morphology in epoxy mirrors that in the D2000 precursor.

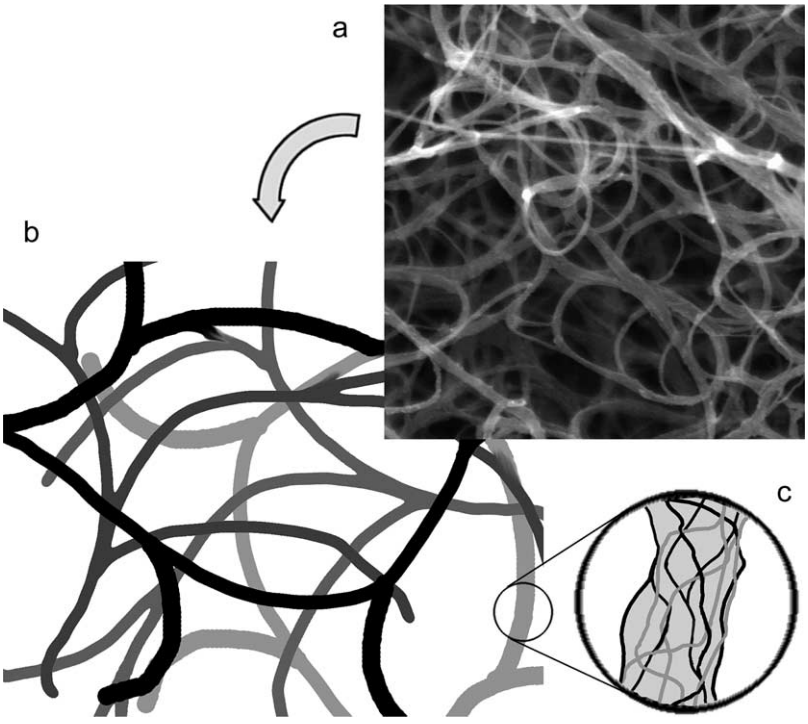

Fig. 15. Schematic of a proposed possible morphology.

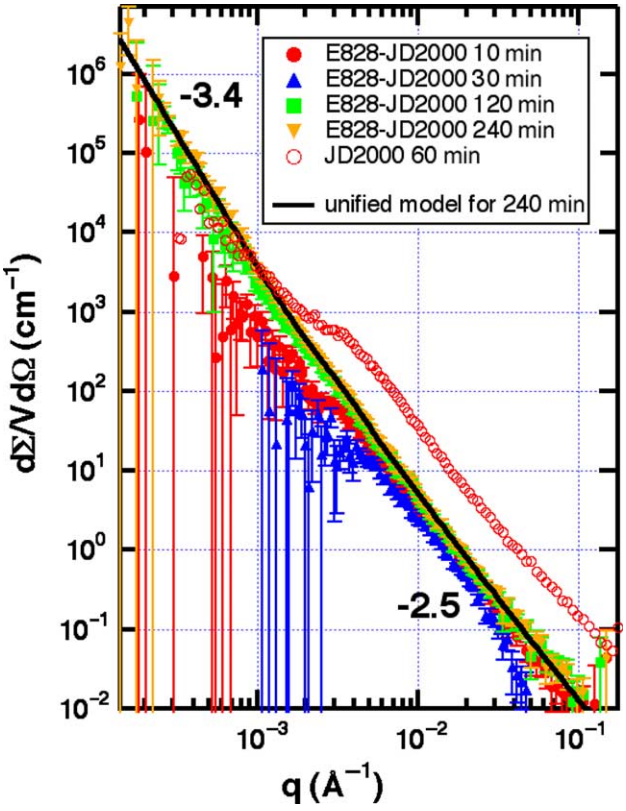

Fig. 16. Background-subtracted USAXS data for Epon 828 cured with SWNT-loaded Jeffamine D-2000. Sonication time refers to the Jeffamine D-2000-SWNT precursor suspension. The data for the Jeffamine D-2000 sample from Fig. 14 are included for comparison.

4. Conclusions

A significantly improved SWNT dispersion method based on sonication of clean unfunctionalized SWNTs in a long chain liquid diamine prior to the addition of epoxy has been developed. The SWNTs are believed to disperse in the diamine due to preferential attraction of the amine for the SWNT and steric stabilization by the long alkyl chain of the D2000. Raman results show that attraction is shown to be relatively weak, not involving covalent bonds.

Despite the effective dispersion of the SWNTS, scattering and light microscopy imply that the SWNTs are not dispersed to the tube level and do not show rod-like behavior on any length scale. Instead the SWNTs remain bundled a hierarchical morphology of SWNTs aggregated into disordered ropes that are further agglomerated into fractal clusters with an average radius of gyration of 1.7 μm. Upon addition of the Epon 828 epoxy and crosslinking, the scattering contrast between SWNT and matrix is significantly decreases but general features of the fractal clusters of disordered ropes persist.

AC electrical measurements confirm the network structure described above. AC electrical measurements indicate that the ropes are percolate below 0.05 wt%.

Acknowledgements

The authors wish to graciously thank Professors Richard Smalley and Robert Hauge for the SWNTs samples and helpful advice. The authors also thank Valerie Moore for several valuable lessons in SWNT suspension preparation. Thanks to Amanda Colleary for many hours of help in sample preparation and light microscopy and to Michael Arlen for many hours of aid and assistance on the Ac spectroscopy. The authors would also like to thank Jefferey Baur helpful advice and very helpful discussions. This research was funded by the Air Force Research Laboratory at Wright-Patterson Air Force Base, Ohio, partially through Prime Contract No.: F33615-00-D-5006 and Subcontract: DO 01 RSC03007 Account No.2387010562.

The UNICAT facility at the Advanced Photon Source (APS) is supported by the US DOE under Award No. DEFG02-91ER45439, through the Frederick Seitz Materials Research Laboratory at the University of Illinois at Urbana-Champaign, the Oak Ridge National Laboratory (US DOE contract DE-AC05-00OR22725 with UT-Battelle LLC), the National Institute of Standards and Technology (US Department of Commerce) and UOP LLC. The APS is supported by the US DOE, Basic Energy Sciences, Office of Science under contract No. W-31-109-ENG-38.

References

[1] Biercuk M, Llaguno M, Radosavljevic M, Hyun J, Johnston A, Fischer J. Appl Phys Lett 2002;80:2767.
[2] Salvetat J, Briggs GA, Bonard J, Basca R, Kulik A. Phys Rev Lett 1999; 82:944.
[3] Ajayan PM, Schadler LS, Giannaris C, Rubio A. Adv Mater 2000;12:750.
[4] Arepalli S, Nikolaev P, Holmes W, Files BS. Appl Phys Lett 2001;78: 1610.
[5] Schaefer DW, Zhao J, Brown JM, Anderson DP, Zhao J, Chokalingam K, et al. Chem Phys Lett 2003;375:369.
[6] Frankland S, Caglar A, Brenner D, Griebel MJ. J Phys Chem B 2002;106: 3046.
[7] Liu T, Kumar S. Nano Lett 2003;3:1379.
[8] Brown JM, Curliss D, Vaia RA. Chem Mater 2000;12:3376.
[9] Park C, Ounaies Z, Watson K, Crooks RE, Smith J, Lowther SE, et al. Chem Phys Lett 2002;364:303.
[10] Bradley K, Gabriel J-C, Briman M, Star A, Gruner G. Phys Rev Lett 2003; 91:218301.
[11] Bradley K, Briman M, Star A, Gruner G. Nano Lett 2004;4:253.
[12] Shim M, Javey A, Kam NWS, Dai H. JACS 2001;123:11512.
[13] Kong J, Dai H. J Phys Chem B 2001;105:2890.
[14] Maeda Y, Kimura S, Hirashima Y, Kanda M, Lian Y, Wakahara T, et al. J Phys Chem 2004;108:18395.
[15] Rouse JH. Langmuir 2005;21:1055.
[16] Lu J, Nagase S, Maeda Y, Wakahara T, Nakahodo T, Akasaka T, et al. Chem Phys Lett 2005;405:90.
[17] Landi BJ, Ruf HJ, Worman JJ, Raffelle RP. J Phys Chem B 2004;108: 17089.
[18] Yang M, Koutsos V, Zaiser M. J Phys Chem B 2005;109:10009.
[19] Moore VC, Strano MS, Haroz EH, Hauge RH, Smalley RE, Schmidt J, et al. Nano Lett 2003;3:1379.
[20] Shvartzman-Cohen R, Nativ-Roth E, Baskaran E, Levi-Kalisman Y, Szleifer I, Yerushalmi-Rozen R. JACS 2004;126:14850.
[21] Chao YC, Shih JS. Anal Chim Acta 1998;374:39.
[22] Kong J, Dai H. J Phys Chem B 2001;105:2890.
[23] Choi N, Kimura M, Katuara H, Suzuki S, Achiba Y, Mizutani W, et al. Jpn J Appl Phys 2002;44:6264.
[24] Furtado CA, Kim UJ, Gutierrez HR, Pan L, Dickey EC, Eklund PC. JACS 2004;126:6095.
[25] O'Connell MJ, Boul P, Ericson LM, Huffman C, Wang Y, Haroz E, et al. Chem Phys Lett 2001;342:265.
[26] O'Connell MJ, Bachilo SM, Huffman CB, Moore VC, Strano MS, Haroz EH, et al. Science 2002;297:593.
[27] Zhang X, Liu T, Sreekumar TV, Kumar S, Moore VC, Hauge RH, et al. Nano Lett 2003;3:1285.
[28] Islam MF, Rojas E, Bergey DM, Johnson AT, Yodh AG. Nano Lett 2003; 3:269.
[29] Richard P, Prasse T, Cavaille JY, Chazeau L, Gauthier C, Duchet J. Mater Sci Eng, A 2003;352:344.
[30] Flandin L, Prasse T, Schueler R, Schulte K, Bauhofer W, Cavaille J-Y. Phys Rev B 1999;59:14349.
[31] Prasse T, Schwartz M-K, Schullte K, Bauhofer W. Colloids Surf, A 2001; 189:183.
[32] Scheuler R, Petermann J, Schulte K, Wentzle H-P. J Appl Polym Sci 1997;63:1741.
[33] Sandler J, Shaffer MSP, Prasse T, Bauhofer W, Schulte K, Windle AH. Polymer 1999;40:5967.
[34] Martin CA, Sler JKW, Shaffer MSP, Schwarz M-K, Bauhofer W, Schulte K, et al. Compos Sci Technol 2004;64:2309.
[35] Sandler JKW, Kirk JE, Kinloch IA, Shaffer MSP, Windle AH. Polymer 2003;44:5893.
[36] Jager K-M, McQueen DH. Polymer 2001;42:9575.
[37] Nikolaev P, Bronikoski MJ, Bradley RK, Rohmund F, Colbert DT, Smith KA, et al. Chem Phys Lett 1999;313:91.
[38] Strong KL, Anderson DP, Ladfi K, Kuhn JN. Carbon 2003;41:1477.
[39] Schaefer DW, Brown JM, Anderson DP, Zhao J, Chokalingam K, Tomlin D, et al. J Appl Crystallogr 2003;36:553.
[40] Beaucage G. J Appl Crystallogr 1995;28:717.
[41] Beaucage G. J Appl Crystallogr 1996;29:134.
[42] Beaucage G, Schaefer DW. J Non-Cryst Solids 1994;172:797.
[43] Dresselhaus MS, Dresselhaus G, Saito R, Raman JA. Phys Rep 2005; 409:47.

[44] Kasuya A, Sigano M, Maeda T, Saito Y, Tohji K, Takahashi H, et al. Phys Rev B 1998;57:4999.
[45] Marcoux PRSJ, Batail P, Lefrant S, Renouuard J, Jacob G, Albertini D, et al. Phys Chem Chem Phys 2002;4:2278.
[46] Corio P, Santos AP, Santos PS, Temperini MLA, Brar VW, Pimenta MA, et al. Chem Phys Lett 2004;383:475.
[47] Fagan SB, Souza Filha AG, Lima JOG, Fihlo JM, Ferrerira OP, Mazali IO, et al. Nano Lett 2004;4:1285.
[48] Chang H, Lee JD, Lee SM, Lee YM. Appl Phys Lett 2001;79:3863.
[49] Heller DA, Barone PW, Swanson JP, Mayrhofer RM, Strano MS. J Phys Chem B 2004;108:6905.
[50] Strano MS, Moore VC, Miller MK, Allen MJ, Haroz EH, Kittrell C, et al. J Nanosci Nanotechnol 2003;3:81.
[51] Park C, Crooks RE, Siochi EJ, Harrison JS, Evans N, Kenik EA. Nanotechnology 2003;14:L11.
[52] Gong X, Baskaran S, Voise RD, Young JS. Chem Mater 2000;12:1049.
[53] Garboczi EJ, Snyder KA, Douglas JF, Thorpe MF. Phys Rev E 1995;52:819.
[54] Rutkofsky M, Banash M, Rajagopal R, Chen J. SAMPE J 2005;41:54.
[55] Barrau S, Demont P, Peigny A, Laurent CC, Lacabanne C. Macromolecules 2003;36:5187.
[56] Stauffer D, Aharony A. Introduction to percolation theory. London: Taylor & Francis; 1992.
[57] Koerner H, Liu WD, Alexander M, Mirau P, Dowty H, Vaia RA. Polymer 2005;46:4405.